ADVANCES IN ATMOSPHERIC SCIENCES, VOL. 25, NO. 5, 2008, 824–839

Sensitivity Study of the Seasonal Mean Circulation in the Northern South China Sea

HONG Bo* (宏 波) and WANG Dongxiao (王东晓)

Laboratory for Tropical Marine Environmental Dynamics, South China Sea Institute of Oceanology, Chinese Academy of Sciences, Guangzhou 510301

(Received 13 September 2007; revised 28 January 2008)

ABSTRACT

A study of the circulation in the northern South China Sea (SCS) is carried out with the aid of a three-dimensional, high-resolution regional ocean model. One control and two sensitivity experiments are performed to qualitatively investigate the effects of surface wind forcing, Kuroshio intrusion, and bottom topographic influence on the circulation in the northern SCS. The model results show that a branch of the Kuroshio in the upper layer can intrude into the SCS and have direct influence on the circulation over the continental shelf break in the northern SCS. There are strong southward pressure gradients along a zonal belt largely seaward of the continental slope. The pressure gradients are opposite in the southern and northern parts of the Luzon Strait, indicating inflow and outflow through the strait, respectively. The sensitivity experiments suggest that the Kuroshio intrusion is responsible for generating the imposed pressure head along the shelf break and has no obvious seasonal variations. The lateral forcing through the Luzon Strait and Taiwan Strait can induce the southwestward slope current and the northeastward SCS Warm Current in the northern SCS. Without the lateral forcing, there is no high-pressure-gradient zonal belt seaward of the continental slope. The wind forcing mainly causes the seasonal variation of the circulation in the SCS. The wind-induced water pile-up results in the southward high pressure gradient along the northwestern boundary of the basin. Without the blocking of the plateau around Dongsha Islands, the intruded Kuroshio tends to extend northwest and the SCS branch of the Kuroshio becomes wider and stronger. The analyses presented here are qualitative in nature but should lead to a better understanding of the oceanic responses in the northern SCS to these external influence factors.

Key words: northern South China Sea, circulation, wind forcing, Kuroshio intrusion, bottom topography

Citation: Hong, B., and D. Wang, 2008: Sensitivity study of the seasonal mean circulation in the Northern South China Sea. *Adv. Atmos. Sci*, **25**(5), 824–840, doi: 10.1007/s00376-008-0824-8.

1. Introduction

The South China Sea (SCS) is the largest marginal sea in the tropics (Fig. 1a). Its deep central basin is bordered by two broad shelf regions to the north and south, each with a water depth of less than 200 m. To the east and west, the continental slopes are very steep, with practically no continental shelf. The northern shelf extends from Taiwan southwestward to 15°N, and averages 150 km in width. The Luzon Strait, with a sill depth of more than 2000 m, connects the SCS with the Pacific Ocean. The intrusion of the Kuroshio through the Luzon Strait has a direct influence on the circulation in the northern SCS.

The upper-layer circulation in the SCS is primarily controlled by the East Asian monsoon. Many international projects have been put in practice in order to better understand the East Asian monsoon and its interaction with the SCS. The South China Sea Monsoon Experiment (SCSMEX) is one of the projects, which provided excellent datasets for studying the interaction of the summer monsoon and the SCS circulation (Ding et al., 2004). Generally, the southwest monsoon prevails from June to September, and a much stronger northeast monsoon takes over from November to March. The wind stress fields show that the northeasterly winds prevail over the whole region during December–February, whereas weaker southeasterly

*Corresponding author: HONG Bo, hongbo@scsio.ac.cn

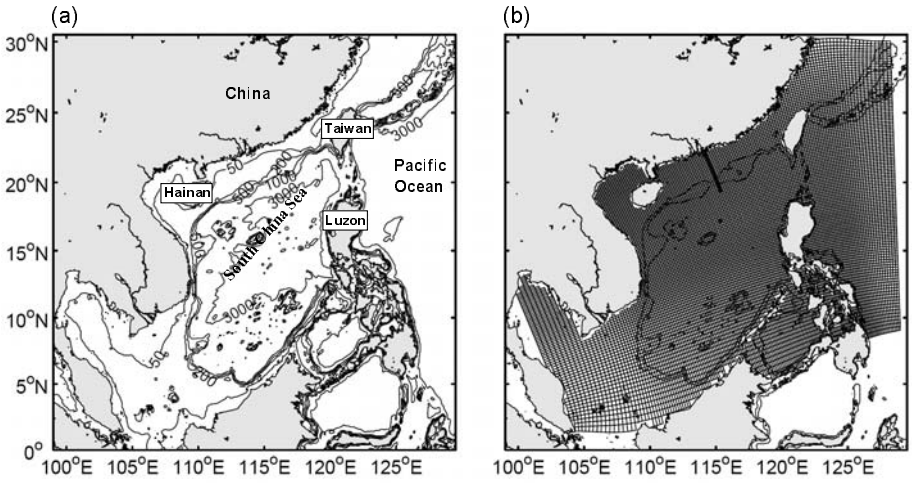

Fig. 1. (a) Bottom topography (m) of the South China Sea and its surrounding regions. (b) The curvilinear orthogonal model grids, superimposed with 200 and 1000 m isobaths. The bold line offshore from the northern SCS coast denotes the across-shelf transect used in analyses.

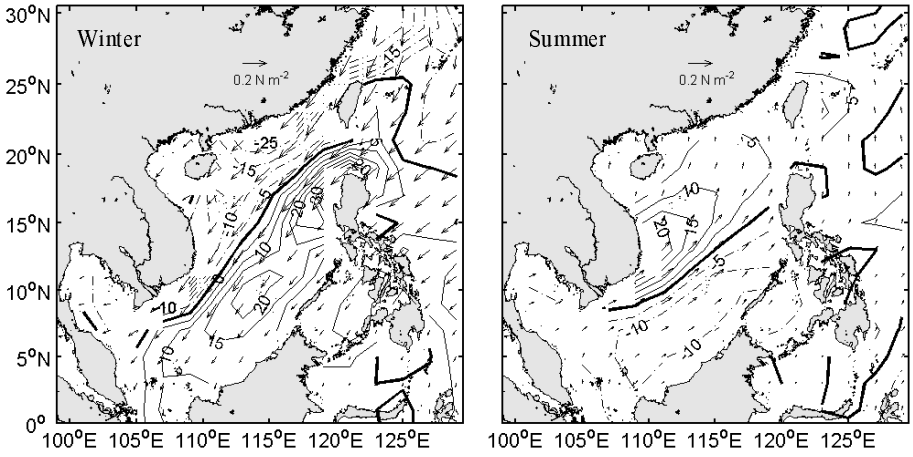

Fig. 2. Climatological wind stress (N m^{-2}) and wind stress curl (10^{-8} N m^{-3}) in winter and summer (after Hellerman and Rosenstein, 1983).

winds occupy most parts of the SCS during June–August (Fig. 2). The seasonal mean circulation of the SCS has been investigated previously (e.g., Wyrtki, 1961; Xu et al., 1982; Li et al., 1996; Fang et al., 1998; Chu et al., 1999; Qu et al., 2000; Cai et al., 2002; Yang et al., 2002; Wei et al., 2003; Xue et al., 2004; Gan et al., 2006). Most of the studies are summarized in a review by Hu et al. (2000). In general, the northern SCS circulation consists of the Guangdong coastal current, the SCS warm current (SCSWC), the slope current, and the meso-scale cyclonic eddy to the northwest of Luzon Island (also called the Luzon Cold Eddy, or LCE). In the upper layers, the northern slope current is called the SCS branch of Kuroshio (SCSBK) by Huang et al. (1992). Some of the features are persistent year round (e.g., SCSWC), whereas others have clear seasonal variations (e.g., LCE).

After having reviewed previous studies, Yang and Liu (1998) concluded that solar radiation, monsoonal wind, and bottom topography could be considered as the main influencing factors for the SCS circulation. In the northern SCS, the influence of Kuroshio intrusion should be added into those factors. Previous studies (e.g., Shaw, 1991; Qu et al., 2000) indicated that, as the northeast monsoon develops in late fall and winter, waters of the North Pacific origin flowed hundreds of kilometers westward along the continental slope of the northern SCS and have a notable impact on the water properties in the entire northern SCS. Qiu et al. (1984) also noted a westward current along the northern SCS continental slope in summer. *In-situ* current measurements of Liang et al. (2003) revealed that a branch of

the Kuroshio intruded steadily and persistently into the SCS; part of the intruded Kuroshio exited the SCS via the northern Luzon Strait and reunited with the main stream of the Kuroshio.

Several studies have noted that the Dongsha Islands has a blocking effect on the westward intrusion of the Kuroshio along the continental slope (e.g., Ma, 1987; Hsueh and Zhong, 2004). Hsueh and Zhong (2004) proposed that the collision of the Kuroshio intrusion with the continental slope near Dongsha Islands could induce pressure head along the continental shelf break. The intruded Kuroshio split into two branches after the collision. The main stream of the intruded Kuroshio veered toward the northeast and eventually exited the SCS through the Taiwan Strait and the northern part of the Luzon Strait, while the remaining part was called the SCSBK.

The combination of surface wind forcing, Kuroshio intrusion, and bottom topographic influence contributes to the complex dynamics of the circulation in the northern SCS. Numerical models can be important tools in helping to separate these dynamics and clarify the contributions of each influencing factor. The purpose of this paper is to qualitatively investigate the effect of different forcing factors on the circulation in the northern SCS through a series of numerical experiments. We focus on the oceanic responses to the influence of local wind forcing, lateral momentum flux, and bottom topography, and analyze the associated seasonal features of these processes.

The model configuration and numerical experiment designs are introduced in section 2. Model-data comparisons are given in section 3. Based on the agreement between the simulations and the observations, model results of a series of experiments are analyzed in section 4 to investigate the responses of the circulation in the northern SCS to different forcing factors. Discussion and conclusions are provided in section 5.

2. Numerical ocean model

The model used in this study is the Princeton Ocean Model (POM). Briefly, the POM is a hydrostatic, free surface, sigma coordinate, primitive equation model, with an embedded turbulence submodel. For an in-depth description of the model and the numerical techniques, the reader is referred to Blumberg and Mellor (1987). Details of the model configuration used in this study are presented below.

2.1 *Model configuration*

In order to introduce realistic Kuroshio dynamic processes at the Luzon Strait, the model domain is extended from the SCS to cover part of the North Pacific and the East China Sea (Fig. 1b). The horizontal grid employs a curvilinear orthogonal system with a variable resolution. Metzger and Hurlburt (2001) suggested that the accurate representation of the north-south island chain within the Luzon Strait is important in modeling Kuroshio intrusion. The use of curvilinear grids allows us to better resolve the regions of steep topography and intense mesoscale variability with relatively less computational load than the rectangular grids. The model grids have higher resolution (about 13 km) in the northern SCS and the western boundary of the North Pacific and lower resolution (about 29 km) in the southern SCS. The ETOP5 data set provided by the National Geophysical Data Center (NGDC) is used to prescribe the model bathymetry through bilinear interpolation. The maximum ocean depth in the model is 5000 m and the minimum depth is 10 m. The vertical sigma coordinate has 30 levels, which are logarithmically distributed with higher resolution near the surface and bottom in order to better resolve the surface and bottom Ekman layers.

The model is initialized with the climatological annual mean temperature and salinity data from the World Ocean Atlas 2001 Boyer et al., 2005) with 0.25° resolution. Surface wind stress is obtained from Hellerman and Rosenstein (1983). A linear restoring scheme of temperature and salinity is used in the upper 5 sigma levels, in which the relaxation time scale is set to be 10 days at the surface and 60 days at level 5. No heat or fresh water flux forcing are applied at the surface since the surface heat and mass exchanges are out of the scope of our sensitivity study.

The lateral forcing is from the simple ocean data assimilation (SODA; Carton et al., 2000) reanalysis products. We use SODA to provide open boundary information for the regional ocean model because it is one of the recognized data sets that have reasonable circulations in the SCS-Pacific region. For example, the annual mean bifurcation point for the North Equatorial Current is around 15°N in the upper layer, comparable with the results of Qu and Lukas (2003). Using the climatological monthly mean values of SODA (averaged over 1992 to 2001), a one-way radiative nesting scheme proposed by Flather (1976) is used for the normal component of the velocity fields. It allows direct connectivity between this regional ocean model and the surrounding circulation, and keeps the same seasonal cycle at each open boundary as that of SODA. A sponge layer, as suggested by Israeli and Orszag (1981), is used for absorbing the unwanted reflections at the open boundaries. The upstream scheme is adopted for the open boundary conditions of temperature and salinity, in which the prescribed values are advected into the model domain for the inflow condition.

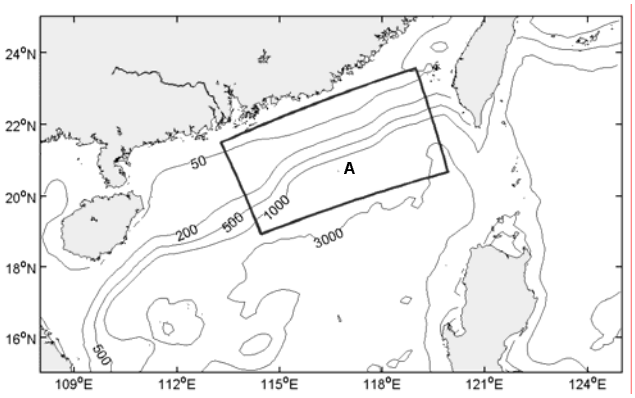

Fig. 3. Bottom topography (m) used in Expt E2. Box A denotes the area in which the plateau around Dongsha Islands is removed along with the island.

Lateral open boundary conditions are very important for a regional ocean model to achieve realistic simulations. The primary rule for a reasonable open boundary condition is, at the first order, the inflow should be balanced by the outflow. We estimated the volume flux through the open boundary of this regional model. In the annual mean, the westward inflow through the eastern open boundary is 33.16 Sv (1 Sv=10^6 m^3 s^{-1}), the southward outflow through the southern open boundary is 28.34 Sv, and the northward outflow through the northern open boundary is 4.34 Sv. Therefore, the inflow is nearly balanced by the outflows.

2.2 *Numerical experiments*

We perform three numerical experiments: one control run, plus two sensitivity runs (Table 1). Experiment E0 (Expt E0) is the control run, in which the surface wind forcing and bottom topography are prescribed. The purpose of Expt E0 is to reproduce the seasonal circulation in the SCS. Sensitivity Expt E1 has zero wind stress forcing during the whole integration, which is aimed at showing the effect of lateral forcing on the circulation in the northern SCS. In Expt E2, we remove the plateau around Dongsha Islands by adjusting and smoothing the bottom topography in box A of Fig. 3, which also shows the modified topography. Expt E2 is used to investigate the influence of bottom topography on the circulation in the northern SCS, especially the path of the intruded Kuroshio.

All experiments are initialized from the resting state with identical lateral boundary conditions. Each experiment includes a 3-year spin-up, followed by 5-year hindcast integration. During the spin-up, the model is forced by the climatological annual mean forcing fields. After that, the model is forced by the climatological monthly mean forcing fields. These forcing fields have been described in detail in subsection 2.1. For each run, the model is integrated under their respective conditions as prescribed in Table 1. Each model year consists of 360 days (30 days per month), and day 1 corresponds to 1 January.

3. Validation of model results

The temporal evolution of the volume-averaged kinetic energy (KE) of the control run indicates that the model has reached statistical equilibrium after the 3-year spin-up (figures not shown). The KE also shows clear seasonal variations over the hindcast integration. The same features of KE exist in the two sensitivity experiments. After the 5-year's hindcast integration, the model has a quasi-equilibrium seasonal cycle. The last year's outputs of all the experiments are believed to be representative of the climatological seasonal circulation in the SCS, which will be analyzed in section 4.

Since Expt E0 aims to reproduce the real seasonal circulation, model validation is only performed for Expt E0. The comparisons between the modeled sea surface elevation fields and those obtained from the T/P altimetry data (averaged from 1993 to 2005) are shown in Fig. 4, after removing the domain-averaged value of each field. In the SCS, the wintertime basin-wide cyclonic circulation and the summertime dipole structure southeast of Vietnam are similar in the model results and the observations. The investigation of Yang and Liu (2003) indicated that there are westward-propagating forced Rossby waves in the northern SCS, with a propagation speed of about 5 cm s^{-1}. The time-longitude diagram of sea surface height

Table 1. Design of the numerical experiments. For each run, the model is integrated from a state of rest under their respective conditions as prescribed below. The lateral boundary conditions are kept identical in all the experiments.

Experiment	Surface wind stress	Bottom topography
E0	Real	Real
E1	Zero surface wind stress	Real
E2	Real	Remove the plateau around Dongsha Islands (by smoothing the bottom topography in the box A of Fig. 3)

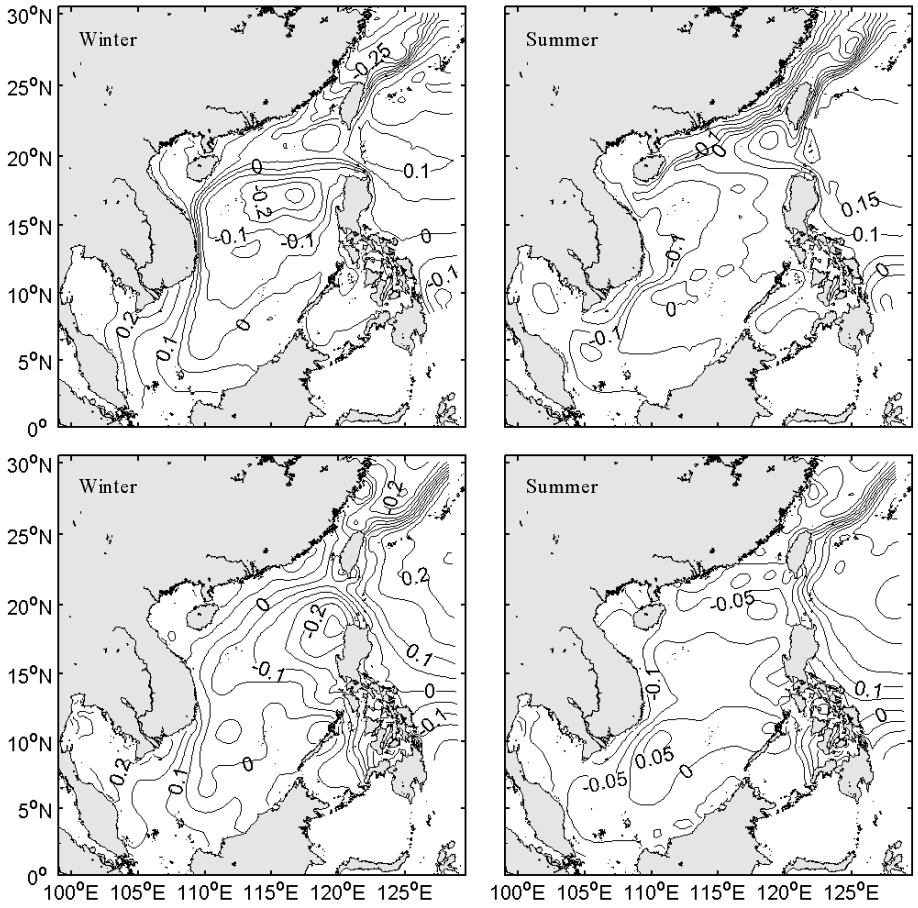

Fig. 4. The modeled (top) and observed (bottom) sea surface elevation fields (m) in winter (left) and summer (right). The observations, which are obtained from the T/P altimetry data, are the seasonal mean of sea surface height from 1993 to 2005. The domain-averaged value is subtracted from each field before the plotting. The contour interval is 0.05 m.

anomaly in the northern SCS from Expt E0 (figure not shown) has a similar pattern to that of Yang and Liu (2003). Analyses of Qu et al. (2004) indicated that the interannual variation of the Luzon Strait transport had an opposite phase compared with the Kuroshio transport east of Luzon, while Kim et al. (2004) showed that the variation of the Kuroshio transport was highly correlated with the North Equatorial Current (NEC) bifurcation latitude. Therefore, reproducing the NEC bifurcation latitude is very important for simulating the Kuroshio intrusion at the Luzon Strait. In the present study, the depth-averaged NEC bifurcation (represented by the zero contours east of the Philippines in Fig. 4) occurs at the southernmost (northernmost) position in summer (winter), with its annual average at about 13°N near the surface. Those features are consistent with the results of Qu et al. (2004) and Kim et al. (2004).

We also compare the annual mean volume transports through the Taiwan Strait, Luzon Strait, Karimata Strait and the transport of the western boundary current of the SCS, Kuroshio east of Luzon Island, and the Mindanao Current with previous studies (Table 2). General agreements exist in terms of exchanges between the SCS and the surrounding waters, and in terms of the transport of the North Pacific western boundary currents. For example, the annual mean volume transport through the Luzon Strait in the model is 5.44 Sv, which is comparable with the result of Metzger and Hurlburt (1996), Qu et al. (2000), and Fang et al. (2005). Actually, estimated volume transport through the Luzon Strait ranges from 8–10 Sv (e.g., Huang et al., 1994) to 2–3 Sv (Wyrtki, 1961). Recently, using current and hydrographic data, Tian et al. (2006) estimated the volume transport through the Luzon Strait to be 63 Sv. More long-term high-resolution observations are needed to obtain more accurate transport through the Luzon Strait. The transport estimated by Wyrtki (1961) is smaller than other studies, which may be a result of the fact that the data

Table 2. Climatological annual mean volume transport (Sv, 1 Sv=10^6 m^3 s^{-1}) of the flows through the Taiwan Strait (TWS), Luzon Strait (LS), Karimata Strait (KS), the western boundary current of SCS (WB), Kuroshio (KU), and Mindanao current (MC). The transport in the eastward (westward) and northward (southward) direction is positive (negative). Rf denotes the reference depth of the dynamic calculations.

Studies	TWS	LS	KS	WB	KU	MC	Notes
Present study	−0.54	−5.44	−2.06	−7.80	25.67	−21.57	
Qu et al. (2000)		−4					
Fang et al. (2005)	0.45	−4.37	−1.32				
Wyrtki (1961)	−0.12	−1.23	−0.45				
Metzger and Hurlburt (1996)		−4.4		−7.7	24.9	−24.8	
Qu et al. (1998)					14	27	Rf 1500 hPa
Toole et al. (1990)					12–31	−14–−30	Rf 1000 hPa
Nitani (1972)					30	−25	Rf 1200 hPa

they used came mainly from surface ship drift and surface wind data. Our transport estimates of Kuroshio and Mindanao Current are very close to those of Nitani (1972) and Metzger and Hurlburt (1996) but not as consistent with the Kuroshio transport obtained by Qu et al. (1998). Such a difference, according to Toole et al. (1990), still lies within the reasonable range of such estimates.

To summarize, these comparisons lend confidence to the success of the model in reproducing the seasonal circulation in the SCS and the success of the open boundary conditions in this regional ocean model.

4. Analysis

4.1 *Seasonal circulation in the northern SCS*

The results of the control run (Expt E0) are used to analyze the seasonal circulation in the northern SCS. The velocity at 50-m depth and sea surface elevation fields are shown in Figs. 5a and 6a, respectively. In winter, the cyclonic circulation is dominant, with a strong slope current flowing southwestwardly along the northwestern continental slope and a mesoscale cyclonic eddy northwest of Luzon Island. A branch of the Kuroshio intrudes into the SCS from the southern part of the Luzon Strait and is blocked by the continental shelf near Dongsha Islands. After the collision, part of the intruded Kuroshio veers northeastward and exits the SCS through the Taiwan Strait and the northern part of the Luzon Strait, while the remaining part continues westward along the continental slope. The northeastward SCSWC is relatively weaker in winter than in the other seasons. There is a high sea surface elevation belt between the SCSWC and the slope current. The northeastward sea surface slope along the southeast China coast is identical to the observations of Fang and Zhao (1989). In summer, there is a relatively weak cyclonic gyre in the deep part of the northwestern SCS. Pohlmann (1987) suggested that this gyre was induced by baroclinic effects. The currents on the continental shelf are strong and consistently flow northeastward. The contours of sea surface elevation on the shelf are largely parallel with the coastline, and the high sea surface elevation belt drops gradually as it extends westward along the outer edge of the continental shelf. Spring and autumn are the transition periods for the region. The SCSWC is strengthened in spring as the wind changes from northeasterly to southwesterly. The simulated circulation pattern agrees rather well with the schematic patterns of Fang et al. (1998) for both summer and winter.

The vertical profiles of the normal velocity along the across-shelf transect in the northern SCS (shown in Fig. 1b) are presented in Fig. 7a. The positive (negative) value corresponds to the northeastward (southwestward) along-shore flow. The seasonal variations of the flow are obvious in the upper 400 m, while the along-slope flow is relatively stable in the deeper layer. In the inner shelf region, the currents show direct responses to the monsoon reversal. The northeastward SCSWC is narrowly confined at the outer edge of the continental shelf in winter and autumn and becomes wider and stronger in spring and summer. There is a year-round northeastward flow around 1400-m depth, whose maximum velocity is larger than 0.1 m s^{-1}. This flow may be related to the outflow of the water from the SCS to the North Pacific through the Luzon Strait, which was noted by Qu et al. (2000) and Tian et al. (2006).

More dynamic insight can be obtained by examining the horizontal pressure gradient fields. Figures 8a and 9a present the horizontal pressure gradient at 50-m depth in the east-west (x) and north-south (y) directions, respectively. The horizontal pressure gradient is defined as

$$\frac{\partial p}{\partial x_i} = \frac{\partial}{\partial x_i}\int_z^\eta \rho g dz' = \rho(\eta) g \frac{\partial \eta}{\partial x_i} + \int_z^\eta g \frac{\partial \rho'}{\partial x_i} dz'$$

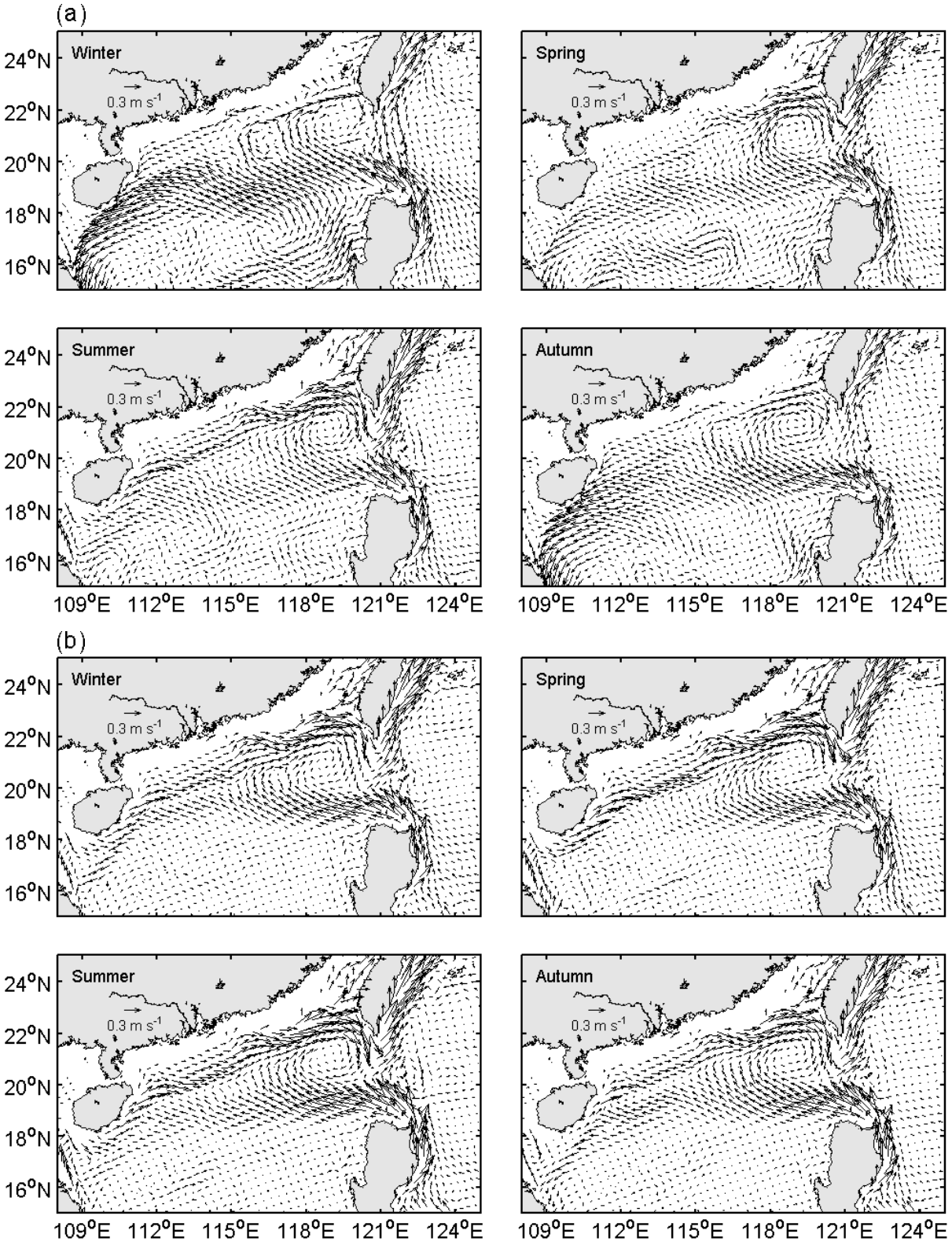

Fig. 5. Seasonal mean velocity fields (m s^{-1}) at 50-m depth for (a) Expt E0 (control run), (b) Expt E1 (without surface forcing), (c) difference between Expts E0 and E1 (Expt E0 minus Expt E1), and (d) Expt E2 (removing the plateau around Dongsha Island).

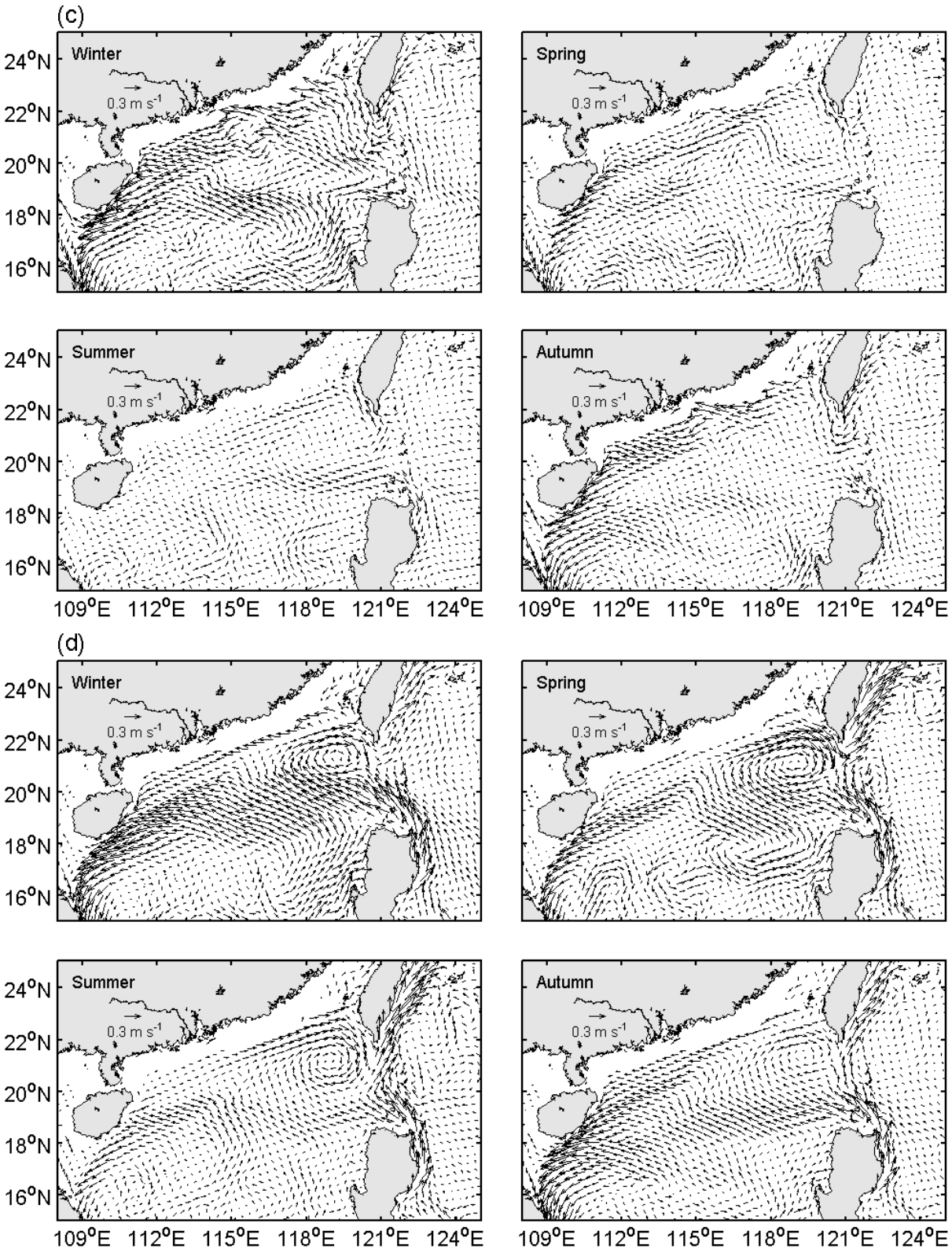

Fig. 5. (Continued).

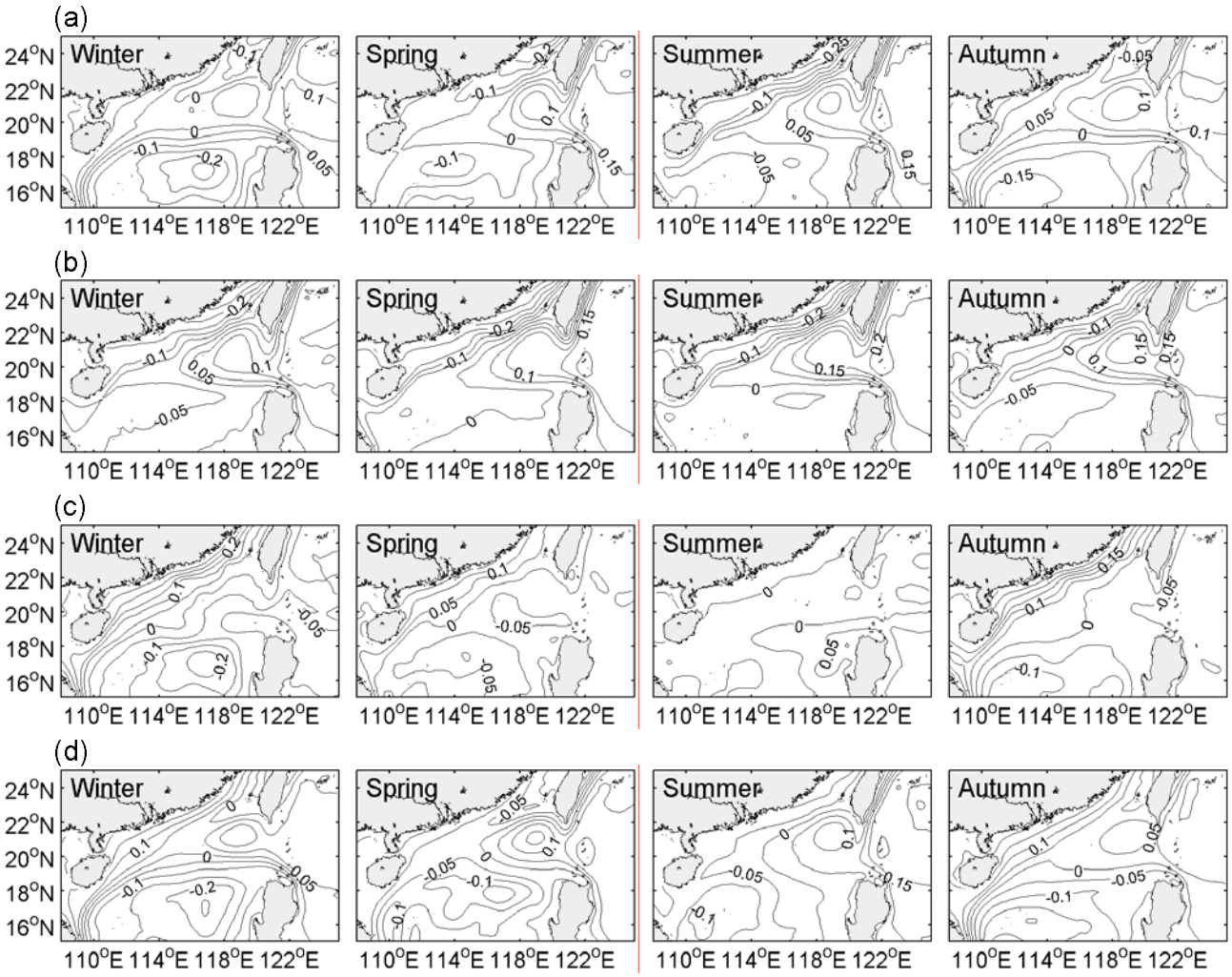

Fig. 6. Seasonal mean sea surface elevation (m) for (a) Expt E0, (b) Expt E1, (c) difference between Expts E0 and E1 (Expt E0 minus Expt E1), and (d) E2, after removing their domain-averaged values. The contour interval is 0.05 m.

where the pressure gradients in x and y directions are represented by the subscripts $i = 1$ and 2, respectively. In the equation, p is pressure, ρ is density, g is gravity, and η is the sea surface elevation. It is well known that there is numerical error in the pressure gradient calculation over a steep topography in the terrain-following ocean model (e.g., Mellor et al., 1998). This numerical error cannot be completely eliminated as long as the grid does not follow geopotential or isopycnal surfaces. In order to reduce this error to an acceptable level (below other numerical errors) several methods have been suggested (e.g., Chu and Fan, 2003; Mellor et al., 1994; Stelling and van Kester, 1994). Among these, three steps are adopted in our calculations. First, the bottom topography is slightly smoothed to remove sharp topographic variations before starting the numerical simulations. Second, the horizontally averaged density has been subtracted from ρ before the calculations, and the remaining part is represented by ρ'. Third, the grid is changed from a sigma grid to a z-level grid before calculating the horizontal pressure gradient. These steps have been proven to be efficient in reducing the pressure gradient error. The westward (eastward) pressure gradient corresponds to the positive (negative) value in Fig. 8a, while the southward (northward) pressure gradient corresponds to the positive (negative) value in Fig. 9a. As Fig. 8a shows, the westward pressure gradients occupy the northeastern SCS throughout the year except in the area southwest of Taiwan Island. The eastward pressure gradients in the northwestern SCS show obvious seasonal variations, which are stronger in winter and autumn than in spring and summer. In the Luzon Strait, the westward pressure gradients are relatively higher in its southern part than that in its northern part. The eastward pressure gradients occupy the region southwest

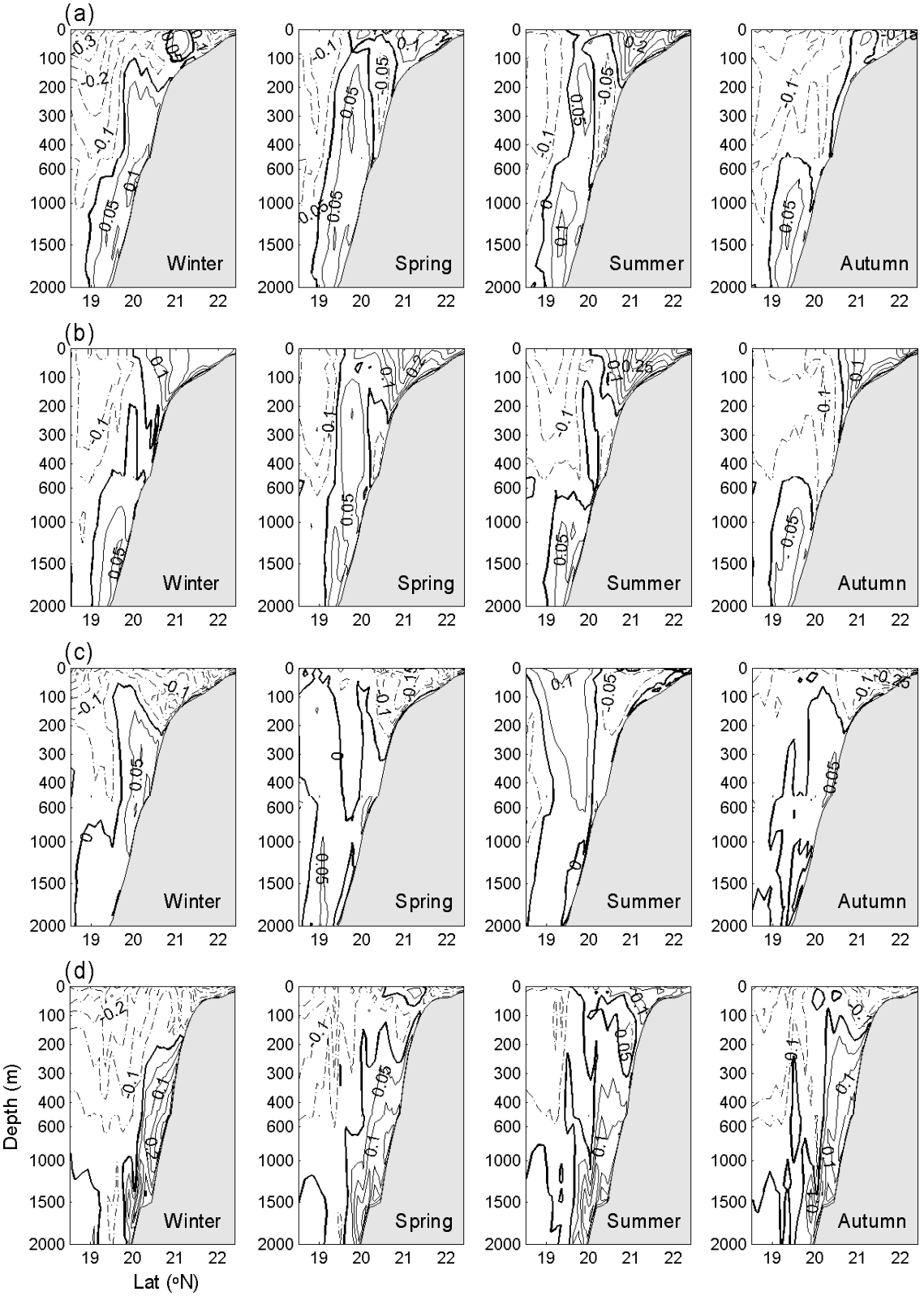

Fig. 7. Vertical profile of the velocity (m s^{-1}) normal to the across-shelf transect in the northern SCS (shown in Fig. 1b) for (a) Expt E0, (b) Expt E1, (c) difference between Expt E0 and E1 (Expt E0 minus Expt E1), and (d) E2. The positive (negative) value corresponds to the northeastward (southwestward) flow. The counter interval is 0.05 m s^{-1}.

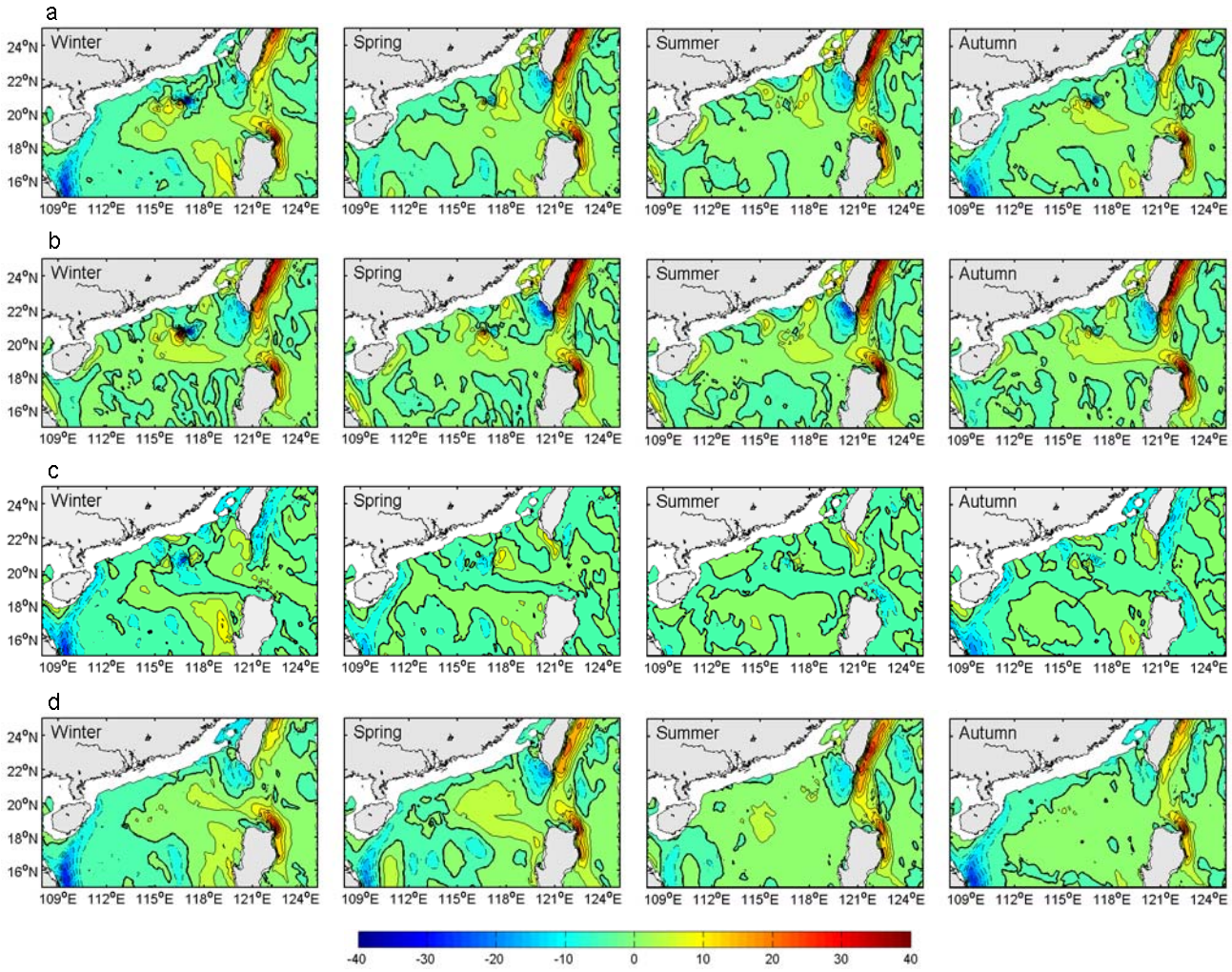

Fig. 8. Fields of horizontal pressure gradients (kg m^{-2} s^{-2}) in the east-west direction at 50-m depth for (a) Expt E0, (b) Expt E1, (c) difference between Expt E0 and E1 (Expt E0 minus Expt E1), and (d) Expt E2. The bold lines are zero contours, and the dashed (solid) lines represent negative (positive) values. The contour interval is 4×10^{-6} kg m^{-2} s^{-2}.

of Taiwan Island all year round, which may be regulated by the topography and intruded Kuroshio water. In Fig. 9a, the southward pressure gradient is dominant along a zonal belt that is largely along the continental slope southwest of Dongsha Islands, whereas the northward pressure gradient occupies the outer edge of the continental shelf with clear seasonal variations. The meridional pressure gradients are opposite in the southern and northern parts of the Luzon Strait, which corresponds to the excursions of Kuroshio in the strait.

4.2 *Effects of lateral forcing*

The lateral forcing through the straits, especially those through the Luzon Strait and Taiwan Strait, has an important effect on the circulation in the northern SCS. For the purpose of qualifying these effects, we use the sensitivity Expt E1 with the forcing only at the lateral open boundary. The velocity at 50-m depth and sea surface elevation fields are shown in Figs. 5b and 6b, respectively. It is shown that without the surface forcing, the circulation south of 18°N is very weak, and the LCE disappears. There is a branch of the Kuroshio that intrudes into the SCS and flows westward along the continental slope all year round. A steady current flows northeastward along the outer edge of the continental shelf, which compares favorably with the observed SCSWC. The vertical profiles of the normal velocity along the across-shelf transect (Fig. 7b) indicates that the SCSWC has an obvious barotropic feature. A high sea surface elevation belt exists between the slope current and the SCSWC, which decreases

from east to west. There are onshore flows between the slope current and the SCSWC, which suggests that the slope current might feed the SCSWC through the onshore flow. This sensitivity run reveals that the high sea surface elevation belt along the continental shelf break may be induced by the Kuroshio intrusion through the Luzon Strait and the outflow through the Taiwan Strait (or lateral forcing through the Luzon and Taiwan Strait), and the generation of the SCSWC is closely related with the SCSBK through the imposed pressure head and the onshore flow in the continental shelf break region. The annual mean Luzon Strait transport in Expt E1 is 5.4 Sv, which is very close to that in the control run (Table 2). This indicates that, although the wind forcing has contribution to the seasonal variation of the Luzon Strait transport, it has little effect on the annual mean Luzon Strait transport. This is consistent with the finding of Metzger and Hurlburt (1996). The transports in the Taiwan Strait, Mindoro Strait, and Karimanda Strait are 1.46, 2.98, and 0.78 Sv, respectively. The inflow and outflow through all the straits are nearly balanced.

From a mass balance point of view, the mean Luzon Strait transport is actually a westward extension of the northern tropical gyre in the West Pacific (Metzger and Hurlburt, 1996). As Fig. 8b shows, the pressure gradient fields in the Luzon Strait calculated from Expt E1 have similar patterns with those from Expt E0. The westward pressure gradient occupies most of the northern SCS. Figure 9b reveals that the southward pressure gradient is relatively stronger in the northeast SCS than that in the northwest SCS, which corresponds to the gradual weakening of the westward flow as it reaches the interior of the SCS. The northward pressure gradients exist consistently on the continental shelf and are quite stable all year round.

4.3 *Effects of wind forcing*

We demonstrate the effect of wind forcing on the circulation by showing the difference between Expts E0 and E1. The differences of the velocity at 50-m depth and sea surface elevation fields are presented in Figs. 5c and 6c, respectively. It is shown that, except to the west of the Luzon strait and the continental shelf break region, the circulations in the northern SCS show similar patterns to those in Figs. 5a and 6a. In winter, the cyclonic gyre occupies the whole basin, and the LCE exists west of Luzon. The Ekman-drift-induced water piles up along the coast, which creates the across-shelf sea surface slope near the coast. The currents in the shallow water flow consistently southwestward. The southwestward SCS western boundary current is maintained in spring and autumn, with meso-scale eddies appearing in the deep sea. These features are mainly the result of wind forcing. It has been shown in previous studies (e.g., Su, 2004) that summer monsoon forces the currents in the northern SCS continental shelf to flow northeastward. However, it can be noted in Fig. 5c that there are almost no leeward (northeastward) currents on the shelf in summer. The vertical profiles of the normal velocity along the across-shelf transect in the northern SCS also reveal that the simulated wind-induced along-shelf flow is very weak in summer. The reason can be explained as follows. As Expt E1 shows, the Kuroshio intrusion can induce a high sea surface elevation belt and the related northeastward current in the continental shelf (Figs. 5b and 6b). Metzger and Hurlburt (1996) suggested that the pressure head created by the pileup of water from the southwest monsoon would reduce the Luzon Strait transport. Without wind forcing, the Luzon Strait transport (which is westward) simulated in Expt E1 is exaggerated in summer, thus, the intruded Kuroshio is stronger than that in Expt E0. Therefore, the circulation in the northern SCS continental shelf/slope simulated in Expt E1 is somewhat overestimated in summer. As a result, the wind-induced circulation obtained from the difference between Expts E0 and E1, is underestimated in summer (Figs. 5c and 6c). The vertical profiles of the along-shelf velocity in the across-shelf transect (shown in Fig. 1b) indicate that the SCSWC totally disappears in this experiment (Fig. 7c).

The wind-induced horizontal pressure gradient fields at 50-m depth are shown in Figs. 8c and 9c, which are in the east-west and north-south directions, respectively. It is shown that there are two high westward pressure gradient regions in the northern SCS: one occurs west of the Luzon Island, the other lies southwest of Taiwan Island (Fig. 8c). The eastward pressure gradients along the northwestern boundary of the basin show similar patterns as those in Fig. 8a, and have obvious seasonal variations. Such variations are consistent with the transition of the monsoon. The pressure gradients in the north-south direction (Fig. 9c) show very different features than those in the other experiments. There is no zonal belt of southward high pressure gradient west of the Luzon Strait. Instead, there are southward high pressure gradients along the northwestern boundary of the basin, which is the result of the water pileup along the northwestern boundary induced by the wind. There is no northward pressure gradient on the northern SCS continental shelf.

4.4 *Effects of bottom topography*

Several studies suggested that the intruded Kuroshio was deflected by the continental slope near Dongsha Islands (e.g., Zhong, 1990; Hsueh and Zhong,

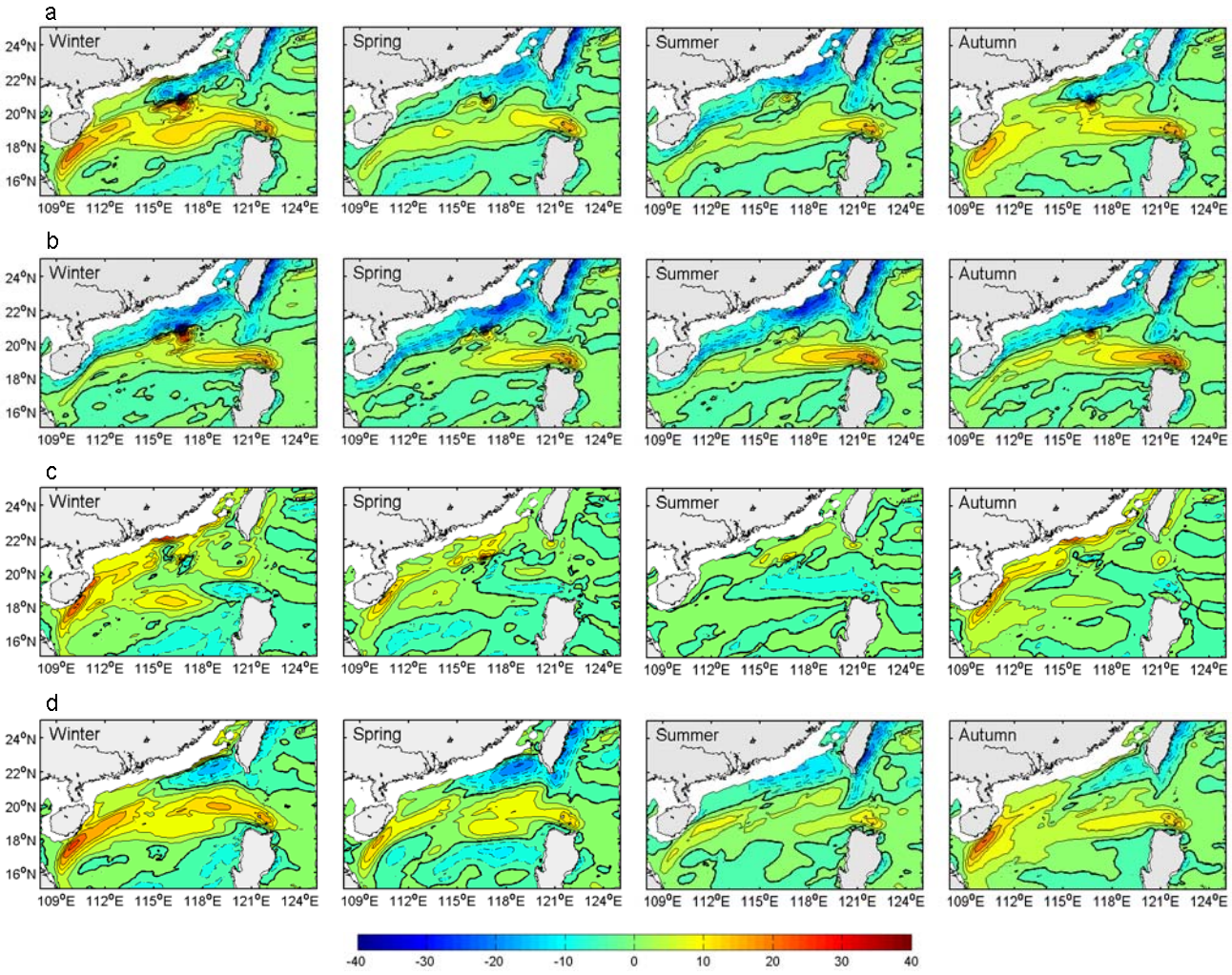

Fig. 9. Same as Fig. 8 but for the fields of horizontal pressure gradient in the north-south direction.

2004). Dongsha Islands lie about 200 km offshore on a plateau over the upper continental slope (Fig. 1a). The intruded Kuroshio is split into two parts after its collision with the continental slope. One part continues westward along the continental slope to form the SCSBK, while the other part is deflected northeastward and eventually exits the SCS through the Taiwan Strait and the northern part of the Luzon Strait. In Expt E2, we remove the plateau around Dongsha Islands (the area defined by box A in Fig. 3) in order to investigate the influence of bottom topography on the northern SCS circulation, especially the path of the intruded Kuroshio. The modified topography is shown in Fig. 3. The velocity at 50-m depth and sea surface elevation fields of Expt E2 are shown in Figs. 5d and 6d, respectively. The intruded Kuroshio shows much tendency to extend westward and the SCSBK becomes wider and stronger. Zhong (1990) proposed that the intruded Kuroshio was deflected in the right-hand tendency owing to the inclination of bottom topography. Such deflection can be explained by the theory of conservation of potential vorticity, or the joint effect of bottom topography and baroclinicity. Comparing Figs. 5a and 5d, we find that, after the modification of topography, the position where the intruded Kuroshio being deflected is modified accordingly. The vertical profiles of the normal velocity along the across-shelf transect in the northern SCS reveal that the SCSWC disappears in winter after modifying the topography (Fig. 7d). Previous investigations have suggested that the SCSBK fed the SCSWC all along the shelf break through a weak onshore flow driven by the gradual drop in pressure in the SCSBK. It can be concluded from this experiment that, without the blocking from the plateau around Dongsha Islands on the intruded Kuroshio, the onshore flow in the continental shelf break region is greatly reduced, especially in winter.

The horizontal pressure gradient fields from Expts E0 (Figs. 8a and 9a) and E1 (Figs. 8b and 9b) show that there are relatively stronger pressure gradients around the Dongsha Islands than elsewhere, especially in winter. In Expt E2, however, such features disappear when the topographic effect around the Dongsha Islands is removed (Figs. 8d and 9d). The relatively strong westward (Fig. 8d) and southward (Fig. 9d) pressure gradients can extend northwestward more easily into the northwestern SCS from the southern part of the Luzon Strait in winter, which indicates that the Kuroshio can intrude northwestward into the interior region of the SCS more easily. The southward pressure gradients along the continental slope seaward of west Guangdong are also strengthened. The pressure gradient fields in the deep sea show little change when compared with the results of the control run.

5. Discussion and conclusions

The combined effects of surface wind forcing, Kuroshio intrusion, and bottom topographic influence result in the complex dynamics of the circulation in the northern SCS. For the purpose of qualitatively investigating the effects of these influencing factors on the circulation, a three-dimensional high-resolution regional ocean model is used in this study in helping to separate these dynamics. The model is forced with climatological monthly mean forcing fields and and is one-way nested in an assimilated global ocean model result, SODA. One control and two sensitivity experiments are performed. The characteristics of the basin-scale circulation in the control run are in good agreement with the observations and previous modeling studies, though some aspects of the results still need to be clarified in the future.

It is well known that the circulation in the SCS is mainly wind-driven, and is regulated by the topography near the continental slope of the basin. Kuroshio intrusion through the Luzon Strait has an important impact on the circulation in the northern SCS. The model results presented in this study indicate that the currents in the inner shelf of the northern SCS have direct response to the monsoon reversal. The northeastward SCSWC is narrowly confined at the outer edge of the continental shelf in winter and autumn, and becomes wider and stronger in spring and summer. The cyclonic gyre exists in the northern SCS all year round, which is consistent with previous studies (e.g., Wang et al., 2000; Wei et al., 2003; Su, 2004). There is year-round northeastward along-slope flow around at a depth of 1400 m in the northern SCS, which may be related to the outflow of the water from the SCS to the North Pacific through the Luzon Strait. So far, there are several viewpoints on the Kuroshio intrusion through the Luzon Strait, such as the intrusion as a direct branch of the Kuroshio (e.g., Liang et al., 2003; Wei et al., 2003), as a loop current (Li and Wu, 1989), or in the form of eddy shedding (Jia and Liu, 2004), etc. As a strong western boundary current, Kuroshio is the primary energy source (either through barotropic or baroclinic instability) for the development and maintenance of mesoscale variability in the Luzon Strait. Studies based on the long-term mean may differ from those based on a synoptic investigation, which may be heavily affected by eddies. This might be the reason why different viewpoints on the Kuroshio intrusion exist. Our present study shows that there is a branch of the Kuroshio intruding into the SCS throughout the year, which is consistent with the composite and moored current observations of Liang et al. (2003).

The results of the sensitivity experiments reveal that the high sea surface elevation belt along the shelf break is mainly induced by the lateral forcing through the Luzon Strait and Taiwan Strait. The Kuroshio intrusion is responsible for generating the imposed pressure head along the shelf break, and the generation of the SCSWC is closely related to the SCSBK through the imposed pressure head and the onshore flow in the continental shelf break region. Such onshore flow can be explained by the conservation of potential vorticity, or the joint effect of bottom topography and baroclinicity. The wind forcing (Ekman drift or Ekman pumping) is responsible for the seasonal variation of the circulation in the SCS. Without wind-induced water pileup, the simulated Luzon Strait transport (in Expt E1) is over-estimated in summer. After removing the plateau around Dongsha Islands (in Expt E2), the intruded Kuroshio shows much tendency to extend westward and the SCSBK becomes wider and stronger. At the same time, the onshore flow between the slope current and the SCSWC is greatly reduced and the SCSWC almost disappears in the across-shelf transect west of the plateau in winter.

The horizontal pressure gradient fields show more dynamic insights of the circulation. There are strong southward pressure gradients along a zonal belt largely seaward of the continental slope. The pressure gradients are opposite in the southern and northern part of the Luzon Strait, which correspond to the inflow and outflow of the water through the strait, respectively. With the lateral forcing only, the northward pressure gradient occupies the continental shelf throughout the year with fewer seasonal variations than in the control run. The wind-induced water pileup results in the southward high pressure gradients along the northwestern boundary of the basin, and there is no zonal

belt of strong southward pressure gradient seaward of the continental slope. When the topographic effect of the plateau around Dongsha Islands is removed, the relatively strong westward and southward pressure gradients can extend northwestward more easily into the interior region of the northern SCS from the southern part of the Luzon Strait in winter. As a result, it is easier for the intruded Kuroshio to extend northwestward into the SCS in this case. Gan et al. (2006) analyzed the momentum balance of the circulation in the SCS. They suggested that the circulation was generally dominated by the geostrophic balance, and that strong ageostrophic component was found associated with the Kuroshio in the Luzon Strait. In this study, the horizontal distribution of the pressure gradients suggests that the SCSBK is merged into the southwestward slope current through the SCS interior circulation gyre. This result supports the view of Fang et al. (2005), Wang et al. (2006), and Yu et al. (2007) that there is a SCS branch of the Pacific-to-Indian Ocean throughflow, which transports water from the Luzon Strait to the Indian Ocean through the SCS.

Knowledge of oceanic responses to the influence of local wind stress forcing, lateral momentum flux, and bottom topography obtained from this study, though qualitative in nature, could provide a better understanding of the dynamics of the circulation in the northern SCS. In the future, the barotropic and baroclinic components of the horizontal pressure gradient should be separated to investigate the momentum budget of the circulation in response to the external forcing. More in-situ measurements are needed to clarify the formation mechanisms of these features.

Acknowledgements. This research was supported by the National Natural Science Foundation of China (Nos. 40625017, 40576013), Scientific Research Foundation of South China Sea Institute of Oceanology, CAS (No. 50601-77), and Natural Science Foundation of Guangdong Province of China (No. 2007A032600002). The altimeter products were produced by SSALTO/DUACS and distributed by AVISO with support from CNES.

REFERENCES

Blumberg, A. F., and G. L. Mellor, 1987: A description of a three-dimensional coastal ocean circulation model. *Three-Dimensional Coastal Model*, Vol. 4, *Coastal Estuarine Studies*, N. Heaps, Ed., American Geophysical Union, Washington, 1–16.

Boyer, T. P., S. Levitus, J. I. Antonov, R. A. Locarnini, and H. E. Garcia, 2005: Linear trends in salinity for the World Ocean, 1955–1998. *Geophys. Res. Lett.*, **32**, L01604, doi:10.1029/2004GL021791.

Cai, S. Q., J. Su, Z. Gan, and Q. Liu, 2002: The numerical study of the South China Sea upper circulation characteristics and its dynamic mechanism, in winter. *Cont. Shelf Res.*, **22**, 2247–2264.

Carton, J. A., G. Chepurin, X. Cao, and B. S. Giese, 2000: A simple ocean data assimilation analysis of the global upper ocean 1950–1995, Part 1: Methodology. *J. Phys. Oceanogr.*, **30**, 294–309.

Chu, P. C., N. L. Edmons, and C. Fan, 1999: Dynamical Mechanisms for the South China Sea seasonal circulation and thermohaline variabilities. *J. Phys. Oceanogr.*, **29**, 2971–2989.

Chu, P. C., and C. Fan, 2003: Hydrostatic correction for sigma coordinate ocean models. *J. Geophys. Res.*, **108**(C6), 3206, doi: 1029/2002JC001668.

Ding, Y. H., C. Y. Li, and Y. J. Liu, 2004: Overview of the South China Sea monsoon experiment. *Adv. Atmos. Sci.*, **21**(3), 343–360.

Fang, G., and B. Zhao, 1989: A note on the main forcing of the northeastward flowing current off the southeast China coast. *Progress in Oceanography*, **21**, 363–372.

Fang, G. H., W. D. Fang, Y. Fang, and K. Wang, 1998: A survey of studies on the South China Sea upper ocean circulation. *Acta Oceanographica Taiwanica*, **37**(1), 1–16.

Fang, G. H., D. Susanto, I. Soesilo, Q. Zheng, F. Qiao, and Z. Wei, 2005: A note on the South China Sea shallow interocean circulation. *Adv. Atmos. Sci.*, **22**(6), 946–954.

Flather, R. A., 1976: A tidal model of the northwest European coneinental shelf. *Memoires de la Societe Royale des Sciences de Liege*, **6**(10), 141–164.

Gan, J., H. Li, E. N. Curchitser, and D. B. Haidvogel, 2006: Modeling South China Sea circulation: Response to seasonal forcing regimes. *J. Geophys. Res.*, **111**, C06034, doi:10.1029/2005JC003298.

Hellerman, S., and M. Rosenstein, 1983: Normal monthly wind stress over the world ocean with error estimates. *J. Phys. Oceanogr.*, **13**, 1093–1104.

Hsueh, Y., and L. Zhong, 2004: A pressure-driven South China Sea Warm Current. *J. Geophys. Res.*, **109**, C09014, doi:10.1029/2004JC002374.

Hu, J. Y., H. Kawamura, H. Hong, and Y. Q. Qi, 2000: A review on the currents in the South China Sea: Seasonal circulation, South China Sea warm current and Kuroshio intrusion. *Journal of Oceanography*, **56**, 607–624.

Huang, Q. Z., W. Z. Wang, Y. S. Li, C. W. Li, and M. Mao, 1992: General situations of the current and eddy in the South China Sea. *Advance in Earth Sciences*, **7**(5), 1–9. (in Chinese with English abstract)

Huang, Q. Z., W. Z. Wang, Y. S. Li, and C. W. Li, 1994: Current characteristics of the South China Sea. *Oceanology of China Seas*, Zhou et al., Eds., Kluwer Academic, 113–122.

Israeli, M., and S. A. Orszag, 1981: Approximation of radiation boundary conditions. *J. Comput. Phys.*, **41**, 115–135.

Jia, Y., and Q. Y. Liu, 2004: Eddy shedding from the Kuroshio bend at the Luzon strait. *Journal of*

Oceanography, **60**, 1063–1069.

Kim, Y. Y., T. Qu, T. Jensen, T. Miyama, H.-W. Kang, H. Mitsudera, and A. Ishida, 2004: Seasonal and interannual variations of the North Equatorial Current bifurcation in a high resolution OGCM. *J. Geophys. Res.*, **109**, C03040, doi: 10.1029/2003JC002013.

Li, L., and B. Y. Wu, 1989: Kuroshio's loop in the South China Sea. *Taiwan Strait*, **8**(1), 89–95. (in Chinese with English abstract)

Li, R. F., D. Guo, and Q. Zeng, 1996: Numerical simulation of interrelation between the Kuroshio and the current of the northern South China Sea. *Progress in Natural Science*, **6**, 325–332.

Liang, W. D., T. Tang, Y. Yang, M. Ko, and W. Chuang, 2003: Upper-ocean currents around Taiwan. *Deep-Sea Res. II*, **50**, 1085–1105.

Ma, H., 1987: On the winter circulation of the northern South China Sea and its relation to large oceanic current. *Chinese Journal of Oceanology and Limnology*, **5**(1), 9–21.

Mellor, G. L., T. Ezer, and L.-Y. Oey, 1994: The pressure gradient conundrum of sigma coordinate ocean models. *J. Atmos. Oceanic Technol.*, **11**, 1126–1134.

Mellor, G. L., L.-Y. Oey, and T. Ezer, 1998: Sigma coordinate pressure gradient errors and the seamount problem. *J. Atmos. Oceanic Technol.*, **15**, 1122–1131.

Metzger, E. J., and H. E. Hurlburt, 1996: Coupled dynamics of the South China Sea, the Sulu Sea, and the Pacific Ocean. *J. Geophys. Res.*, **101**, 12331–12352.

Metzger, E. J., and H. E. Hurlburt, 2001: The importance of high horizontal resolution and accurate coastline geometry in modeling South China Sea inflow. *Geophys. Res. Lett.*, **28**(6), 1059–1062.

Nitani, H., 1972: Beginning of the Kuroshio. *Kuroshio: Its physical aspects*, H. Stommel and K. Yoshida, Eds., University of Tokyo Press, Tokyo, 129–163.

Pohlmann, T., 1987: A three dimensional circulation model of the South China Sea. *Three-Dimensional Models of Marine and Estuarine Dynamics*, J. Nihoul and B. Jamart, Eds., Elsevier Science, 245–268.

Qiu, D., T. Yang, and Z. Guo, 1984: A westward current in the northern South China Sea in summer. *Tropical Oceanology*, **3**, 65–73. (in Chinese)

Qu, T., 2000: Upper-layer circulation in the South China Sea. *J. Phys. Oceanogr.*, **30**, 1450–1460.

Qu, T., and R. Lukas, 2003: The bifurcation of the North Equatorial Current in the Pacific. *J. Phys. Oceanogr.*, **33**, 5–18.

Qu, T., H. Mitsudera, and T. Yamagata, 1998: On the western boundary currents in the Philippine Sea. *J. Geophys. Res.*, **103**, 7537–7548

Qu, T., H. Mitsudera, and T. Yamagata, 2000: Intrusion of the North Pacific waters into the South China Sea. *J. Geophys. Res.*, **105**, 6415–6424.

Qu, T., Y. Y. Kim, M. Yaremchuk, T. Tozuka, A. Ishida, and T. Yamagata, 2004: Can Luzon Strait transport play a role in conveying the impact of NESO to the South China Sea? *J. Climate*, **17**, 3644–3657.

Shaw, P. T., 1991: The seasonal variation of the intrusion of the Philippine Sea water into the South China Sea. *J. Geophys. Res.*, **96**, 821–827.

Stelling, G. S., and J. A. T. M. van Kester, 1994: On the approximation of horizontal gradients in sigma coordinates for bathymetry with steep bottom slope. *International Journal for Numerical Methods in Fluids*, **18**, 915–935.

Su, J. L., 2004: Overview of the South China Sea circulation and its influence on the coastal physical oceanography outside the Pearl River Estuary. *Cont. Shelf Res.*, **24**, 1745–1760.

Tian, J., Q. Yang, X. Liang, L. Xie, D. Hu, F. Wang, and T. Qu, 2006: Observation of Luzon Strait transport. *Geophys. Res. Lett.*, **33**, L19607, doi:10.1029/2006GL026272.

Toole, J. M., R. Millard, Z. Wang, and S. Pu, 1990: Observations of the Pacific north equatorial current bifurcation at the Philippine coast. *J. Phys. Oceanogr.*, **20**, 307–318.

Wang, D., Q. Liu, R. X. Huang, Y. Du, and T. Qu, 2006: Interannual variability of the South China Sea throughflow inferred from wind data and an ocean data assimilation product. *Geophys. Res. Lett.*, **33**, L14605, doi:10.1029/2006GL026316.

Wang, L. P., C. J. Koblinsky, and S. Howden, 2000: Mesoscale variability in the South China Sea from the TOPEX/Poseidon altimetry data. *Deep-Sea Res.*(*I*), **47**, 681–708.

Wei, Z., G. Fang, B. Choi, Y. Fang, and Y. He, 2003: Sea surface height and transport stream function of the South China Sea from a variable-grid global ocean circulation model. *Science in China* (*D*), **46**(2), 139–148.

Wyrtki, K., 1961: Physical oceanography of the Southeast Asian waters. *Naga Report*, **2**, 1–195.

Xu, X. Z., Z. Qiu, and H. C. Chen, 1982: The general descriptions of the horizontal circulation in the South China sea. *Proc. 1980 Symposium on Hydrometeorology of the Chinese Society of Oceanology and Limnology*, Science Press, Beijing, 137–145. (in Chinese with English abstract)

Xue, H., F. Chai, N. Pettigrew, D. Xu, M. Shi, and J. Xu, 2004: Kuroshio intrusion and the circulation in the South China Sea. *J. Geophys. Res.*, **109**, doi: 10.1029/2002JC001724.

Yang, H. J., and Q. Liu, 1998: A summary on ocean circulation study of the South China Sea. *Advance in Earth Sciences*, **13**, 364–368.

Yang, H. J., and Q. Liu, 2003: Forced Rossby wave in the northern South China Sea. *Deep-Sea Res.*, **50**, 917–926.

Yang, H. J., Q. Liu, Z. Liu, D. Wang, and X. Liu, 2002: A general circulation model study of the dynamics of the upper ocean circulation of the South China Sea. *J. Geophys. Res.*, **107**(C7), doi:10.1029/2001JC001084.

Yu, Z., S. Shen, J. P. McCreary, M. Yaremchuk, and R. Furue, 2007: South China Sea throughflow as evidenced by satellite images and numeri-

cal experiments. *Geophys. Res. Lett.*, **34**, L01601, doi:10.1029/2006GL028103.

Zhong, H. L., 1990: Density-related current structures. *Report of 10-year Hydrographic Section Surveys of the Northern South China Sea Continental Shelf Region and Adjacent Waters*. China Ocean Press, Beijing, 215–241. (in Chinese)